ABSTRACT

Title of Thesis: *QUANTUM DOT ENCAPSULATED VIRAL LIKE PARTICLES BASED ON ADENO-ASSOCIATED VIRUS*

*Matthew James Wolpert, Master of Science, 2020*

Thesis Directed By: Assistant Professor, Gregg Duncan, Bioengineering

Adeno-associated virus (AAV) has emerged as a leading gene-therapy candidate due to its broad tissue tropism and encouraging safety profile. Traditionally, viral biodistribution is assessed through expression of reporter genes in tissues days to weeks post-vector administration. This does not provide insight into how AAV initially distributes throughout the body which will impact its effectiveness and long-term safety. Towards this end, we optimized a strategy for assembling a viral like particle (VLP) using capsid proteins from AAV serotype 2 and incorporated a quantum dot (QD) into its core. Their uptake was visualized in human embryonic kidney (HEK) cells *in vitro*. Our findings enable further optimization of VLP-QD systems for AAV biodistribution analysis. In addition, extracellular vesicles (EVs) are a new class of gene-delivery vector with potential in pulmonary disease. We measured the diffusion of EVs from two cell lines in human mucus to determine their potential as an inhaled therapeutic.

# QUANTUM DOT ENCAPSULATED VIRAL LIKE PARTICLES BASED ON ADENO-ASSOCIATED VIRUS

by

Matthew James Wolpert

Thesis submitted to the Faculty of the Graduate School of the
University of Maryland, College Park, in partial fulfillment
of the requirements for the degree of

Master of Science

2020

Advisory Committee:

Professor Gregg Duncan, Chair

Professor Steven Jay

Professor Tao Lowe

## Acknowledgements

I would like to sincerely thank Dr. Duncan for his mentorship over these last couple of years. He has, without a doubt, provided me amazing guidance and made my time in his lab very enjoyable. There is no way my project would have made much progress had it not been for his weekly input (or sometimes daily on ‘slack’).

I would also like to thank my lab-mates and friends, who helped me talk through experiments when things weren’t working, or even to take my mind off science in times of stress. But, most importantly, they set a great example with their incredible work ethic that kept me motivated and focused. Special thanks to Logan, for helping me so much throughout the editing process!

I would like to offer special thanks to the Jay lab for providing us with EVs and to Stephanie, in particular, for performing the EV characterization experiments. Additionally, thanks to the Huang lab and Clyne lab, for sharing lab supplies with me post-quarantine while everything I needed was backordered!

Thank you to my family, for being so supportive and for listening (or at least staying on the phone) as I told you about my experiments and went into far too much detail about what I had been up to.

Lastly, thank you so much to my wife, Margaret, who emotionally and financially supported me through graduate school and whose love and support made grad school that much easier.

# Table of Contents

# Table of Figures

## Significance and Motivation

AAV is a leading *in vivo* gene therapy candidate due to its mild immune response, its ability to transduce a variety of cell types and its stably expressed episomal gene product. Understanding its biodistribution soon after administration could provide useful knowledge to enhance its already appealing traits. Quantum dots (QDs) have been used in many different *in vivo* imaging applications, including for biodistribution and to obtain high intensity fluorescence images with low amounts of background[1]. By incorporating QDs directly into the capsid of a virus, it will be possible to obtain better insight into the cellular uptake process *in vitro* and the real-time biodistribution of the virus *in vivo*. Similar work has been done using Brome mosaic virus, a similar non-enveloped, icosahedral virus, which indicates it may be also possible with the AAV capsid[2]. There has been some success incorporating QDs into the viral capsid, however, the only study to do so with AAV used well-established EDC-NHS chemistry to attach it onto the outside of the capsid[3]. While this can still be effective for following the AAV uncoating process *in vitro*, a 25% increase in diameter could significantly alter how the particles move in a complex, 3D biological system.

# Chapter One: Background

## Viral-Based Gene Therapy: Adeno-Associated Virus

### *Gene Therapy*

Gene therapy has become a promising technology to supplement or correct a defective gene in place of treating symptoms throughout a patient's life. There are many ways to deliver a gene into a host nucleus, such as using a non-viral vector to deliver CRISPR-cas9, transcription activator-like effector nucleases (TALENs) or zinc-finger nucleases (ZFNs), which can be effective however they suffer from low efficiency[4,5]. Viral vectors, on the other hand, have an innate ability to hijack cellular machinery to generate complex proteins using their genome as a template and they require no extra technology to aid in gene transfer. Viruses have gained traction due to their natural ability to infect a variety of cell types and their engineered potential to evade the complex human immune system.

Worldwide, there are 3704 ongoing clinical trials using gene therapy, with viruses dominating the majority of recent successes. Of the viral based gene therapies 34% use a retrovirus (RV), 32% use Adenovirus (AdV), 10% use Herpes Simplex Virus (HSV) and 24% use Adeno-Associated Virus (AAV)[6]. In 2017, the first AAV-based gene therapy, Luxterna, was FDA approved to treat patients with RPE65-associated Leber Congenital Amaurosis, an inherited disorder that causes blindness. The FDA has since released a report reducing the stringency of approval for viral-based gene therapies, which will significantly increase the number of emerging viral-based drugs[7]. Of the viruses capable of delivering a corrective gene, most have been retroviral (RV), meaning they carry a single stranded RNA genome and must be transcribed into DNA via reverse transcriptase before insertion to the

host genome. Most RV drugs must be used *ex-vivo* due to the difficulty of restricting insertion events *in vivo,* which can result in side effects such as cancer[6]. Although they have become limited to *ex vivo* usage, they are actually far superior for those purposes because they integrate into the host genome allowing for long term expression in dividing cells[8]. AAV, on the other hand, is more suitable for *in vivo* usage because of their mild safety profile and their ability to stably express episomal DNA in non-dividing cells[9].

*Adeno-Associated Virus*

AAV was originally discovered in a preparation of Simian AdV that was initially thought to be contaminated[10]. It was soon realized that AAV was its own virus and was simply replication defective. In regard to gene therapy, it has become a particularly good alternative to other viruses because of its low pathogenicity. It also has a variety of naturally occurring serotypes and it rarely, but predictably, inserts into the host's genome at AAV integration site 1 (AAVS1) on Chromosome 19. It is a non-enveloped parvovirus with a capsid 22nm in diameter. The genome is a single strand of DNA (ssDNA), 5kb in length with one inverted terminal repeat (ITR) on each end. The genome is made up of two genes, *rep* and *cap*. *Rep* encodes for Rep78, Rep68, Rep52 and Rep40 (named from their approximate molecular weights) from a single open reading frame (ORF). The two larger rep proteins, Rep78 and Rep68, are necessary for replication and have endonuclease and ATP-dependent helicase function[11]. The smaller two rep proteins, Rep52 and Rep40, act as motor proteins that package the newly synthesized genome into mature AAV capsids[12,13]. The three capsid proteins (CP) are translated from the *cap* gene and are designated VP1, VP2 and VP3. They are regulated by the combination of a rare start codon (ACG) and alternative splicing, causing the VP1 and VP2 proteins to have the same amino

acid sequence as VP3 at their C-terminus. The mature AAV capsid is comprised of 60 CPs in a 1:1:10 ratio (VP1:VP2:VP3) held together in icosahedral geometry. The subunits form 2-fold, 3-fold and 5-fold axes of symmetry with a depression located along the 2-fold axis, 3 protrusions surrounding a depression on the 3-fold axis and a small channel located at the center of the 5-fold axis (**Figure 1.1**)[14]. AAV can be fully formed and packaged by only using VP2 and VP3 CPs, however it requires VP1 for successful gene expression[15].

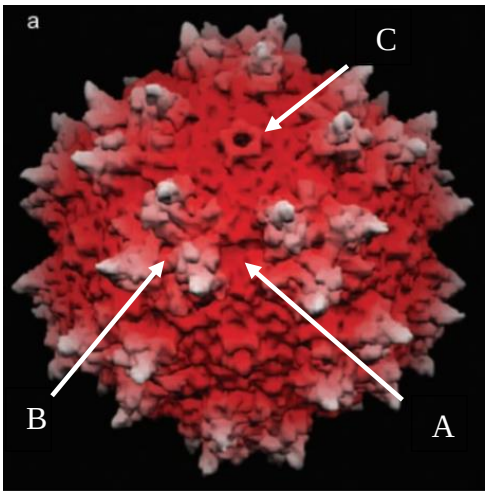


**Figure 1.1: Capsid surface symmetry of AAV2[16]. A)** Shows the 2-fold axis of symmetry **B)** shows the 3-fold axis of symmetry and **C)** shows the 5-fold axis of symmetry.

*Cell Entry*

Currently there are 12 known naturally occurring serotypes of AAV, each using a different combination of primary and co-receptors. Most serotypes use sialic acid, heparin sulfate or galactose as their primary receptors and are subsequently endocytosed. They can enter using clathrin-independent carriers and GPI-anchored-protein-enriched endosomal compartments however each serotype has a slightly different method of entry[17,18]. As the

late-endosome is carried closer to the nucleus, the acidification process alters the conformation of CPs VP1 and VP2, which exposes their N-terminus. The N-terminus of VP1 has been shown to have phospholipase activity and is required for successful infection of AAV[19]. The intact AAV virions then can escape from the late-endosome and accumulate in the peri-nuclear region of the cell. The virions then translocate into the nucleus, the genome is released, and second strand synthesis can begin. The ssDNA is first converted into a double-stranded template, a process initiated by the ITRs, which allows the genome to be transcribed or inserted into AAVS1[20]. Of the entire AAV genome, the only regions necessary for efficient transgene expression are the ITRs[21]. Since they only make up 4% of the genome, the remaining 96% can be replaced with a therapeutic transgene, which must include a promotor and a poly-A tail.

*Transgene*

The design of a therapeutic gene cassette is essential for optimizing protein expression and function. Many studies have been done to optimize the ITR sequence due to their essential roles in cell transduction and propagation. Until the genome is double stranded it cannot undergo transcription, thus, prohibiting translation and subsequent protein production. This rate-limiting step can be bypassed by introducing a mutation into one of the ITRs by removing the binding motif of Rep78 and Rep68, which prevents them from induce second strand synthesis. Instead, the wild-type and mutated ITR form a circular, self-complementary genome that is capable of priming its own second strand[22]. The main drawback of self-complementary AAV's (sc-AAV) is that they must include the plus and minus strands of DNA making this method impractical for transgenes larger than 2.5kb. Splitting the transgene into two or many distinct recombinant AAV (rAAV) allows for

expression for a larger transgene than by using a single rAAV. It takes advantage of homologous recombination (HR) that occurs from the presence of overlapping ITRs[23,24]. Recombination specific sequences can also be added to the ends of random transgene fragments to induce recombination at more specific locations. This optimizes the recombination events to promote the formation of a final product that is a completely intact transgene larger than 5kb[25].

*Immune Response*

The human body can mitigate AAV infection by preventing cell-entry through capsid recognition, recognizing the viral DNA inside the cell or recognizing the products of transcription/translation of the viral transgene[26]. The two main roadblocks to successful transduction of AAV are neutralizing antibodies (NAbs) and cytotoxic T lymphocytes (CTLs). NAbs help prevent the initial binding of AAV to its primary receptor by recognizing and binding to specific motifs on the AAV capsid. This has proven to be very difficult to overcome because as much as 50% of the population already has NAbs for many of the wild-type AAVs (wt-AAV)[27]. Another cellular response to AAV infection when the capsid has any exposed tyrosine residues on its capsid. The tyrosine is phosphorylated, and ubiquitinated, followed by degradation by the proteasome[28]. After degradation, the individual AAV CPs are processed through the transporter associated with antigen processing (TAP), which allows these capsid fragments to be bound by major histocompatibility complex (MHC) class I molecules and subsequently transported to the cell surface[29,30]. When MHC class I molecules are present on the cell surface, CTLs recognize this signal and destroy the infected cell.

The last possible immune response to AAV is when the cell identifies the therapeutic transgene expression as foreign. This can happen when the host's disease is one caused by a deletion mutation, where the introduction of the newly synthesized peptide sequence is considered "unknown" and is targeted by CD8+ T cells, thus, undoing the successful delivery of a therapeutic protein[31]. Because these immune responses rely on recognizing a specific motif on the viral capsid or the binding of specific, well-characterized molecules, many of these responses can be evaded by the utilization of an engineered capsid or can be reduced by the addition of other small molecules that interfere with the cellular response pathways.

An easy pathway to target to interfere with is the proteasome-based degradation pathway. By using an already FDA approved proteasome inhibitor, the ubiquitylation of the capsid can be blocked, which allows a higher concentration of AAV to be trafficked into the nucleus rather than degraded[32]. Many other approved small molecules have been identified through high-throughput screening methods; many of which are topoisomerase inhibitors that induce host DNA damage[33]. The increased DNA damage may "distract" the cellular machinery away from the viral DNA long enough to allow the majority of ssDNA to become dsDNA. Inhibition of many DNA damage pathways has been linked to AAV transduction enhancement, however the exact mechanism remains unknown[34,35].

*Capsid Engineering*

Many different methods have proven successful in evading neutralizing antibodies. Cell targeting peptides have become an easy way to change the primary receptor AAV uses to enter the cell. This can be done by replacing residues on VP1, forcing different amino acids to be exposed on the surface[36,37]. By doing this, the rAAV capsid is undetectable to NAbs

because the motif they recognize would no longer be present. The main drawback of this method is that it can significantly alter receptor binding affinity. However, by using this method in conjunction with an uptake assay, the AAV capsid modifications that are successfully transduced can be isolated and obtained.

Using random peptide libraries, instead, relies on the introduction of random mutations rather than the change in selected residues. After the generation of an rAAV library with many random mutations, random peptide rAAVs are added to cells *in vitro*. The rAAV that are successfully transduced are characterized and subsequently cataloged to then be used for transgene delivery[38]. The third approach uses the *cap* gene from multiple serotypes produce a variation of CPs. When capsid assembly begins *in vitro,* proteins from all added serotypes come together to form a polyploid capsid[39]. Instead of having many binding sites per particle for NAbs to recognize and a single primary receptor, particles can enter cells via multiple primary receptors and better evade the NAbs already present[39].

The last method, directed evolution, can be done using three different approaches: *in silico*, *in vitro* or *in vivo*. *In silico* uses computational modeling to identify protein fragments that have no effect on the 3D structure of the capsid in order to ensure proper folding and functionality[40]. The *in vitro* approach utilizes a genome shuffling technique, usually error-prone PCR or a random genome insertion, to introduce random mutations into the AAV capsid with subsequent rounds of transduction, harvesting and amplification. It is also possible to include an incubation step with NAbs to select against a potential immune response. After many rounds, the rAAV capsid will be altered to minimize NAb recognition and maximize transduction of the chosen cell type[41]. The *in vivo* approach uses the same concept as *in vitro*, however the process selects against the host's immune

response as well. After the target tissue is harvested, the AAV sequence can be amplified and purified[42]. This method has been successfully used to administer a truncated form of the cystic fibrosis transmembrane regulator (CFTR) to a porcine knock-out model after multiple rounds of selection[43].

*In vitro Production*

To successfully generate mature rAAV capsids *in vitro*, a cell line requires co-infection with another virus, typically AdV or HSV. The cultured cells are typically ones that grow very quickly such as HeLa or HEK293. The process includes transfecting the cells with 3 plasmids that contain a therapeutic gene of choice flanked by the 2 ITRs, the *rep* and *cap* genes, and the helper-virus genes that induce viral replication. Once mature rAAV are produced, the culture medium is collected, and the rAAV are subsequently purified. This process consists of sucrose, CsCl or Iodixanol gradients, and various types of chromatography (affinity, ion exchange, size exclusion, etc.). Depending on the chemistry of the capsid, one method may be more advantageous than another. By using 3 sperate plasmids rather than a single plasmid, each can easily be modified separately and systematically to engineer novel AAV strains and to manipulate the AAV genome to elucidate the unknown biological processes of AAV.

*Adeno-Associated Virus Assembly*

AAV assembly is believed to take place in the nucleolus, however the exact mechanism has yet to be elucidated[44]. By using a Pulse-Chase technique, Myers and Carter showed that AAV2 makes empty capsids very quickly and that the rate-limiting step of forming a fully functional AAV2 particle lies with the rate of genome insertion[45]. Once the intact

capsid leaves the nucleolus, its replicated genome can then be inserted through the combination of the large rep proteins interacting with the capsid and the smaller rep proteins acting as a motor to insert the ssDNA through one of the pores located at a 5-fold axes of symmetry[46].

In 2010, a '+1' frameshifted ORF was identified in the Cap gene of AAV2 that coded for a 204 amino acid protein called Assembly Activating Protein (AAP)[47]. An AAP has been found in all other AAV serotypes and contains many conserved residues; it is deemed essential for nearly all serotypes[48]. To determine AAPs role in assembly, Naurer et al. 2012 introduced an early stop codon into the reading frame of AAP from AAV2 (AAP2) such that it had no effect on potential downstream alternate start codons and was upstream of essential amino acids[49,50]. The stability of the capsid proteins was assessed *in vitro* by inhibiting the proteasomal degradation pathway with and without AAP. Without AAP, CPs were degraded by proteasomal degradation, however after adding AAP back *in trans*, AAV capsid assembly was almost completely rescued to its wild-type titer[50].

Until recently, all assembly related work with AAP-CP interactions had been done with VP3-only capsids. When similar AAP2 knock-out experiments were performed using all AAV CPs, it was determined that AAP2 was indeed essential for AAV2 CP stability and assembly *in vitro*, however each serotype has its own AAP with slightly different nuclear localization signals[51]. It was later determined that some serotypes have nucleolar or nuclear localization signals, while others were found in both locations[52]. This study hinted at the fact that AAPs function has more to do with protein stability than nuclear transportation because it was performed in mammalian and insect cultures side-by-side and each had the same results[52].

### *Investigating Transgene Delivery*

Currently the most commonly utilized methods to test for rAAV transduction *in vitro* are by fluorescence detection after reporter transgene expression or by using a qPCR-based assay. *In vitro*, these methods are easily performed by putting infected cells under a fluorescent microscope or by assessing mRNA levels after a simple lysing step. While these methods may also be used *in vivo*, they are considerably more difficult. In many cases, the animal must be sacrificed to isolate the target tissue prior to fluorescent detection. There has been some success in a non-invasive viral detection method using firefly luciferase. After viral transduction, the IVIS system (Perkin Elmer) can be used to assess bioluminescence after luciferin injection[53]. As powerful as this method is, the fluorescence can only be detected after the luciferase enzyme is expressed and cannot give any indication of the real-time biodistribution of the virus.

## Viral-Like-Particle Assembly

### *Viral Assembly*

Viruses such as Tobacco Mosaic Virus (TMV) or Brome Mosaic Virus (BMV) have basic capsids consisting of multiple copies of the same subunit. Because they have "simple" capsids, it is possible to take the disassembled individual capsid building blocks and assemble functional viral like particles (VLPs) with capsids and transduction comparable to the wild type[54,55]. This can be achieved in a test tube either by increasing the number of capsid subunits above a critical concentration or by dialyzing against a buffer with favorable assembly conditions[56,57]. Unlike pathogenic viruses, there has been little scientific demand to research AAV's assembly mechanism. However, due to its recent

success in clinical trials, a better understanding of its intracellular assembly processes has become necessary to help minimize self-inhibitory effects from genetic alterations introduced from capsid engineering.

*Methods of Viral Assembly Around Quantum Dots*

Because of their appealing optical properties, QDs have started to be utilized in a variety of bioimaging techniques. Of the many methods of QD attachment, one of great appeal is the internal labeling of viral capsids. There have been a number of published studies done to generate VLP-QD hybrid particles; each has used a slightly different approach. The most common of these approaches was done by first disassembling the capsid, then removing the nuclei acids. This step is followed by a second round of dialysis with a lower ionic strength buffer causing the protein dimers to reassemble. Although dialysis has been used to reassemble many different viruses, incorporation of a quantum dot has only been done in a few, the first being BMV. Dixit et. Al showed that during the reassembly step, QDs can be combined with the individual proteins in order to be encapsulated by the newly formed VLPs[2]. A similar method was also done with canine parvovirus, another non-enveloped, icosahedral virus. The only difference with their method was that they made the viral proteins in *E. coli* rather than disassembling the intact canine parvovirus to obtain them[58].

The second of these methods relies on changes in concentration to initiate VLP formation rather than manipulation of buffer conditions. This work was performed using the MS2 bacteriophage, whose capsid disassembles into basic dimers. Various concentrations of dimers were filtered through a 100 kDa membrane to identify the concentration at which yielded the majority of capsids rather than dimers[59]. By simply combining QDs with a

concentration of MS2 dimers above their critical concentration, it was possible to encapsulate QDs into the core of the resulting VLPs[60].

## Therapeutic Nanocarriers: Extracellular Vesicles

### *Extracellular Vesicles*

Extracellular vesicles (EV) are a heterogeneous population of lipid membrane vesicles released from most cells and play a huge role in cell-cell communication[61]. They can be categorized into three different subgroups based on their origin (**Figure 1.2)**. Apoptotic bodies are the result of controlled cell death and are between 1µm and 5µm. The second largest are microvesicles and are formed by the outward budding of the plasma membrane to form vesicles 100nm-1µm in diameter. The smallest of the vesicles are exosomes, which are between 30nm and 150nm. They were first discovered in 1983 budding off of maturing reticulocytes, however, they have been found in many different types of bodily fluids since then[62][63]. Exosomes originate in the late endosome as it begins its inward budding process, leading to the formation of multivesicular bodies (MVB). Cytosolic macromolecules and proteins are internalized by the newly forming vesicles. As the MVB fuse with the cell membrane, its vesicular contents are released outside of the cell as exosomes[64].

EVs, in particular, have become a vehicle of interest due to their natural ability to hold cargo such as proteins, lipids, mRNA and non-coding RNA depending on their donor cell-type. They have also had success in targeting tumors, due to the abundant expression of the same ligands and receptors as their donor tumor cells[65].

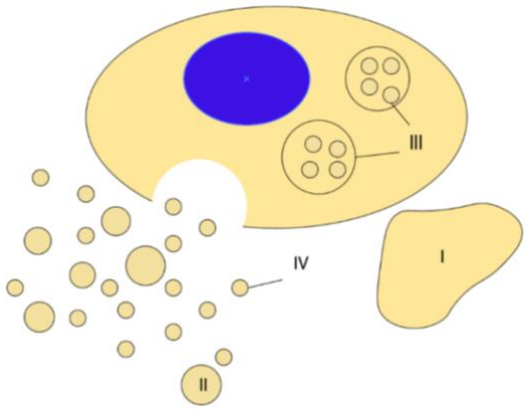


**Figure 1.2: Schematic of EV formation.** Depiction of the formation of an apoptotic body (I), mivrovesicles (II), multivesicular bodies (III) and exosomes (IV).

*Extracellular Vesicle Production and Purification*

EVs are typically isolated from conditioned media that is first collected and then processed through a series of centrifugation steps to remove large particulates. Following the first step, many aggregates and larger vesicles still remain, requiring the use of a density gradient. Although this method can be effective, a filtration step is commonly used at the end to maximize purity. Because of the overlapping size and density ranges of the different types of vesicles, most procedures end up isolating a heterogenous population of EV.

EVs commonly carry specific proteins such as cluster of differentiation (CD) molecules which can be used to help characterize the newly isolated population[66]. These molecules are used in immunophenotyping and play important roles in cell signaling and cell adhesion. By using these molecules, EVs can be targeted by antibodies conjugated to a resin or a magnetic bead as an alternative method of purification; however, it is important to recognize that other cellular particles could also contain the target CD protein[67].

*Extracellular Vesicles as Nanocarriers*

The hydrophilic core of EVs makes it possible to engineer them to carry biologically active molecules (**Figure 1.3**). The majority of the EV's cargo comes from its donor cell, therefore it is vital to use a cell type that will not interfere with the intended result; the donor cell type can have drastic effects on the fate of the EV. For example, mouse tumor derived EVs (Td-EV) isolated *in vitro* and then transferred on to human dendritic cells have been shown to gain a potent tumor antigen response[68]. However, other studies have shown that Td-EVs also play a role in tumor metastasis[69]. These polar-opposite responses illustrate the importance of the cargo, depending on the tumor cell of origin and the possible downstream effects on metastasis and the immune system. Although the response of Td-EVs is difficult to predict, further characterization has given them an emerging role as a tumor diagnostic[70]. The monitoring of micro-RNA (miRNA) levels, in particular, has become powerful in recognizing various diseases due to the ease of PCR-based methods and how readily accessible EVs are in many parts of the body[71]. Not only do they have potential in diagnostics and tumor targeting, in 2007 EVs were observed to deliver mRNA from a host cell to a neighboring cell, which was subsequently translated into a functional protein[72].

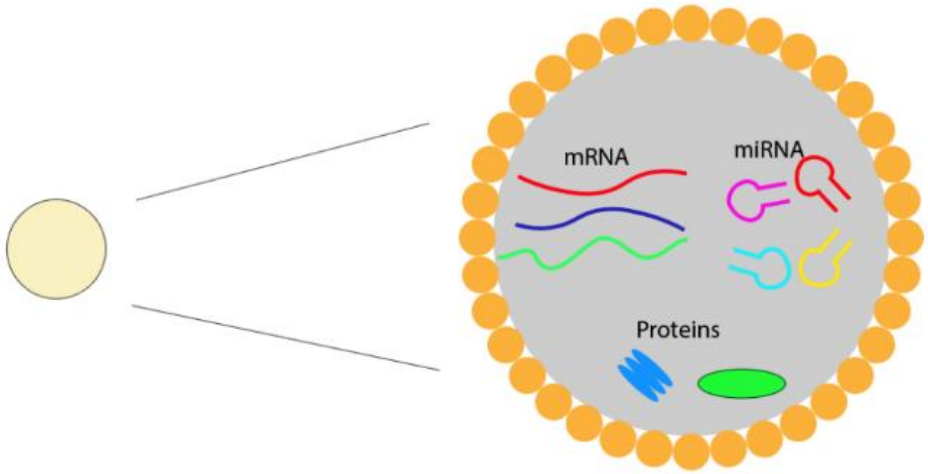


**Figure 1.3: Schematic of the potential cargo of an EV**

*Therapeutic Loading of Extracellular Vesicles*

They have appealing qualities as a nanocarrier; however, they are only as effective as their drug loading efficiency. Each method has its benefits and drawbacks; however, some are still preferred over others. Simple diffusion relies on a drugs ability to diffuse through the membrane to satisfy the concentration gradient. This slow and imprecise method is only possible for drugs that can penetrate its lipid bilayer. Because EVs are typically harvested from a donor cell line, it is also possible to add the drug directly to the culture medium allowing it to be taken up by the cells; thereby, the EVs produced already contain the drug. Although these methods are easy to perform, it is not possible to load cargo such as small-interfering RNA (siRNA) or miRNA, which are too large to diffuse through the membrane. These small, non-coding RNA molecules are important in many biological processes, most importantly, they interact with the RNA-induced silencing complex[73]. This complex seeks out its target mRNA and silences translation via endonuclease activity[74].

The active loading techniques are very effective but also much more disruptive to the membrane. Sonication is an appealing method because of its efficiency and practicality;

however, the drug can attach onto the membrane as well as inside the vesicle, giving the EV an unintended dual-phase drug release. Extrusion is by far the most disruptive method for the membrane and consists of pushing the drug and EV mixture through a porous membrane (100nm-400nm) with a syringe. Electroporation is another method capable of loading siRNA and miRNA. Electroporation uses an electric field to disturb the integrity of the membrane causing small pores to appear. The opening of these pores allows for the drug to flow into the core of the EV in a way that minimizes membrane disruption. Although this method is widely used, it can lead to RNA or EV aggregation. By optimizing the electroporation buffer, these effects can be minimized[75]. A new, appealing way to load EVs is by using a pH gradient. By using a pH gradient, non-coding RNA molecules were loaded successfully into purified EVs at comparable concentrations to electroporation and sonication without the use of any external energy to disrupt the membrane[76]. EVs have the potential to efficiently penetrate through the mucus barrier, as they play in important cell-cell signaling role and navigate through complex 3D biological systems on a regular basis.

# Chapter Two: Quantum Dots Encapsulated by Viral like Particles Based on Adeno-Associated Virus

## Introduction

The field of gene therapy has been rapidly growing given its possibility to treat an abundance of diseases[77]. AAV, especially, has emerged as a leading gene delivery vector because of its naturally occurring serotypes with the ability to target a variety of tissues and its minimal immune response. Given the variety of tissues the naturally occurring AAV serotypes can target, it is important to understand what happens to them directly after administration, and before they reach their intended target. Traditionally, the location of AAVs, once administered *in vivo,* only becomes known upon expression of a fluorescent reporter gene[78–80]. Waiting for a reporter to be expressed can take days to weeks, which makes fluorescent labeling an appealing approach. However, if this type of approach were attempted *in vivo* using a dye, the fluorescence intensity would be far too low for real-time measurements. Fluorescent labeling generally only works *in vitro* however, a capsid fully saturated with dye or nanoparticles dragging behind may significantly affect their natural surface and how they react in a biological environment.

The convenient optical properties of CdSe quantum dots (QDs) provide the ability to achieve single particle resolution *in vitro* and increased resolution *in vivo* due to their inherent brightness and long-lasting photostability[81,82]. These benefits make it advantageous to incorporate them into bio-imaging techniques, and more importantly, into the imaging of gene-delivery vehicles, to better assess particle location in real-time.

Previous studies have incorporated QDs into viral capsids to form viral like particles (VLP-QDs), however this has yet to be done with AAV[83–87]. Although a QD has successfully been attached to the outside of an AAV capsid for cellular uptake observation, a 25% increase in particle size at the nanoscale can significantly alter how it behaves in solution, not to mention a biological landscape[3]. Another study encapsulated Brome Mosaic Virus (BMV), a 25nm icosahedral, non-enveloped virus, with a QD by first disassembling the capsid and reassembling the capsid proteins around the QDs in suspension [85]. The newly assembled virus or VLP, closely resembles the wild-type virus (wt-virus) containing the same capsid proteins. Although VLPs can differ structurally from the wt-virus, they can still provide valuable insight into its behavior.

We sought to incorporate a single QD into a VLP made of AAV2 capsid proteins to gain the ability to assess biodistribution in real-time. This work has the potential to provide insight into AAV circulation time and real-time distribution of AAV in tissues. This protocol initially used for BMV, was adapted for AAV to insert a single QD into its core to provide the optical benefits of a QD while maintaining the surface integrity of the AAV2 capsid.

## Materials and Methods

*Assembly of AAV2 VLP-QD's*

The AAV2 CMV-Null virions were acquired from Vector Biolabs (Cat 7026). The intact AAV2 virions ($2.5x10^{12}$ vg/mL) were first disassembled by performing dialysis against 500mM $CaCl_2$ solution at 4 °C for 24h. All dialysis steps were performed using slide-a-lyzer mini dialysis devices (10kDa MWCO) against 200mL buffer. The ssDNA was

removed by centrifugation at 16,000 x g for 20 min at 4 °C. The supernatant containing the disassembled capsid subunits was dialyzed against 10mM Tris, pH 7.4 for 24h at 4 °C to remove residual calcium ions. The surface of the QDs used in all experiments were functionalized with carboxyl groups. QDs with emission maximums at 605nm and 525nm were used (Thermo Fisher). To encapsulate the QDs with the capsid subunits, a 2:1 ratio of QDs to AAV was combined and dialyzed against reassembly buffer (50mM Tris + 50mM NaCl + 1mM KCl + 5mM $MgCl_2$, pH 7.4) at 4 °C for 24h. The assembled VLP-QDs were then filtered by using .5mL Amicon Ultra filter units (100kDa MWCO) and reconstituted in PBS to concentrate and to remove unassembled materials. The concentrated VLP-QDs were stored at 4 °C for downstream analysis.

*Quantification of ssDNA*

After removal of the supernatant containing the capsid subunits, the resulting DNA pellet was reconstituted in 30uL ultra-pure $H_2O$ and quantified using a Nanodrop 2000c.

*Transmission Electron Microscopy*

Electron micrographs were taken using a JEOL JEM 2100 transmission electron microscope operated at an accelerating voltage of 110kV, equipped with a CCD camera. 5uL of VLP-QD sample was applied to a plasma cleaned carbon coated copper grid (cat cu-300HD, pacific grid tech) for 10 min. Excess sample was removed using filter paper followed by 4, 45sec wash steps with ultra-pure $H_2O$. The grid was negatively stained with 5uL of Uranyl Acetate Replacement Stain (cat. 22405, Electron Microscopy Sciences) for 30 min using a 4x dilution followed by 4, 45sec wash steps with ultra-pure $H_2O$. The grid was placed in a petri dish sealed with parafilm to dry overnight.

*Dynamic Light Scattering*

Dynamic Light Scattering (DLS, Brookhaven Omni) was used to determine the reassembly of AAV VLPs in the absence of QDs. In preparation for DLS, samples were dialyzed against 10mM NaCl for 24h at 4 °C.

*Quantification of VLP-QD*

VLP-QDs were quantified using Spark Multimode Microplate reader. The fluorescence intensity of VLP-QDs was compared to a standard curve of known quantities of QDs to estimate the concentration of the VLP-QD sample.

*Cellular Uptake*

Uptake experiments were performed using human embryonic kidney (HEK) cells because it has been demonstrated they readily express heparin sulfate proteoglycan (HSPG) which acts as the main receptor to AAV2 [88]. HEK cells were seeded onto coverslips and left overnight to attach. QDs ($2.4x10^{11}$ QD/mL) or VLP-QD ($2x10^{9}$ VLP/mL) were combined with fresh cell medium and incubated on HEK ceclls for 3 hours. Cells were then fixed in 4% formaldehyde for 10 minutes followed by staining with Hoechst at a concentration of 2µg/mL for 15 minutes followed by a PBS wash. Coverslips were then mounted on glass slides and imaged on a Zeiss 800 LSM microscope equipped with a 20x objective. Because Hoechst and QDs both excite in similar ranges, the QDs were imaged on a cy3 channel as they have a much wider excitation range than Hoechst.

## Results and Discussion

### *Virion Disassembly*

In order to verify the disassembly of AAV2, we quantified the ssDNA after dialysis against 500 mM $CaCl_2$. Two different amounts of AAV2, $5x10^{10}$ viral genomes (vg) and $1.5x10^{11}$ vg were disassembled and centrifuged to isolate the ssDNA. The average amount of ssDNA obtained in the $5x10^{10}$ vg preparation was 49.57±28.2 ng and the average ssDNA obtained in the $1.5x10^{11}$ vg preparation was 143±9.9 ng, consistant with a 3x increase in number of AAV2 (**Figure 2.1A)**. The estimated DNA amount for the $5x10^{10}$ vg and $1.5x10^{11}$ vg preparations were 32.75 ng and 98.25 ng, respectively. Given that the isolated DNA was quantified using a Nanodrop, the overestimation in concentration and large standard deviation is consistent with previously published data[89]. The total amount of measured ssDNA for each preparation was compared to a calculated estimate from the molecular weight and length of the AAV2-ITR's combined with the Cytomegalovirus (CMV) promoter, multiplied by the number of particles.

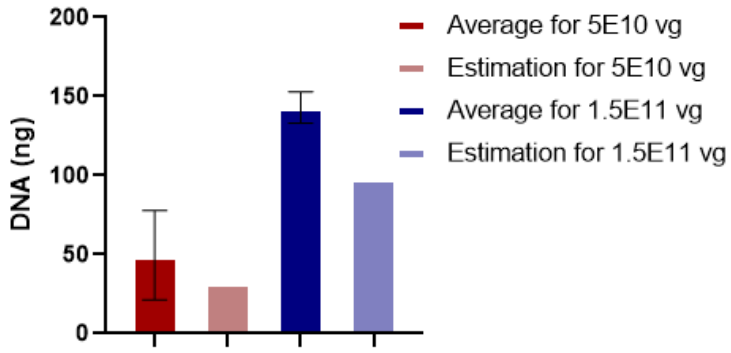


**Figure 2.1: Verification of the disassembly of AAV2. A)** Quantification of DNA obtained from AAV2 after dialysis against 500 mM $CaCl_2$.

*Reassembly*

After verification of virion disassembly, reassembly conditions were then evaluated. Reassembly was first attempted without the presence of QDs to ensure formation of spherical VLPs before addressing QD encapsulation. Reassembly buffer was prepared using a range of KCl concentrations: 1 mM, 10 mM, 50 mM, and 100 mM. This range was chosen to attempt to mimic the intracellular concentrations of $K^+$ and $Cl^-$, ~140mM and ~4mM, respectively[90]. Reassembly was measured after dialysis against reassembly buffer for 24 hours followed by dialysis against 10 mM NaCl to prepare the sample for DLS. Five DLS measurements were recorded for each condition, and the average of all measurements was plotted (**Figure 2.2A).** The mode diameters for the conditions were 26.25 nm, 44.89 nm, 8.19 nm, and 14.54 nm for 1 mM, 10 mM, 50 mM, and 100 mM KCl, respectively.

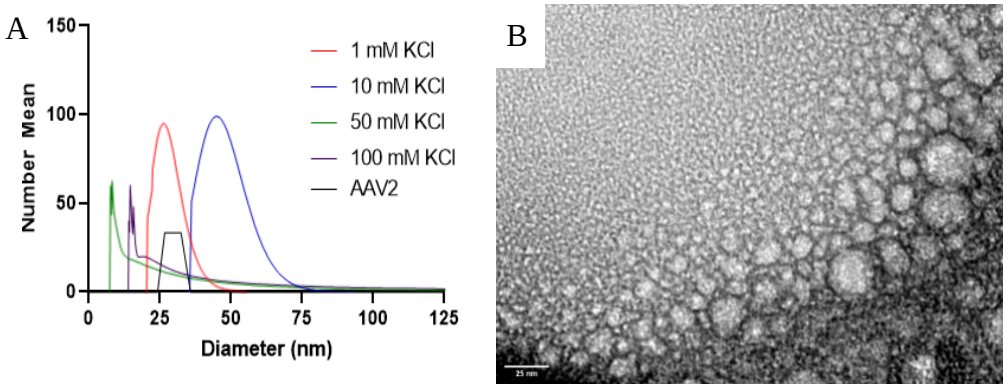


**Figure 2.2: Analysis of reassembled VLPs. A)** size distribution determined by DLS using reassembly buffers with varying ionic strengths **B)** TEM image of reassembled VLP in 1 mM KCl. Scale bar represents 25 nm.

Although the mode diameters of the 50 nm and 100 nm KCl buffers appear very small, the mode diameters of each individual measurement were inconsistent, indicating the formation of larger protein aggregates amongst smaller protein globules. Based on these

data, it was determined that reassembly buffer containing 1 mM KCl generated the most reproduceable VLPs that were closest in size to AAV2. At 1mM KCl, VLP assembly was likely due to electrostatic interactions, because as ionic strength is increased a 'shielding effect' is generated which allows protein-protein and Van der Waals forces to dominate. This is consistent with previous work using cowpea chlorotic mottle virus (CCMV), a 28nm non-enveloped, icosahedral virus, which observed formation of smaller VLPs while using a lower ionic strength buffer; they determined that a decrease in ionic strength lead to the formation of smaller VLPs and was mainly driven by electrostatic interactions, whereas an increased ionic strength lead to formation of larger VLPs driven by protein-protein interactions[91]. The reassembled VLPs were then imaged using transmission electron microscopy (TEM) to verify the DLS data (**Figure 2.2B)**.

*Reassembly around Quantum Dots*

After the verification of the size and shape of the VLPs using DLS and TEM, reassembly of VLPs with QDs was performed using two different QDs, with an emission maximum of 605 nm (QD605) and 525nm (QD525). When the QD605s were used, the VLP size closely resembled that of AAV2, however it was difficult to determine whether the QD605s were attached or partially encapsulated (**Figure 2.3A)**. It was determined that increasing the image contrast could help solve this problem because traditionally it is difficult to image a biologic substance using TEM without the presence of a heavy-metal stain such as uranyl acetate. To achieve this, uranyl acetate replacement stain was added to the same grid imaged in Figure 2.3A and, as expected, the contrast of the image was improved (**Figure 2.3B)**. Even though it was easier to identify the outline of the individual VLPs, the QDs still appeared to be attached to the capsid rather than inside their core. Rather than

optimizing reassembly with the QD605s, QD525s were used instead, because QDs with smaller emitting wavelengths also have a smaller diameter[92]. After this small change, VLPs encapsulating single QD525s were observed (**Figure 2.3C)**. The use of QD525s also significantly decreased the number of free QDs after purification using 100kDa MWCO spin filter, reinforcing the notion that QD525s had a smaller diameter than QD605s. A high magnification image was also taken to help identify the spherical VLP capsid around the dense, black QD525 (**Figure 2.3D)**. Further optimization of stain time and concentration is necessary, as the VLPs should have a distinct white ring around the QD[93].

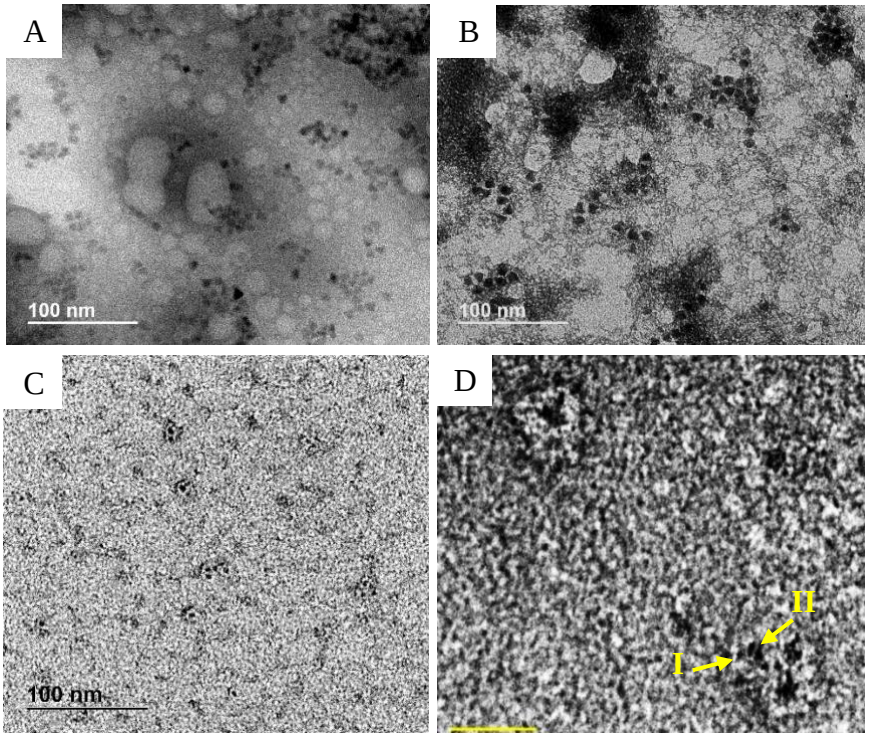


**Figure 2.3: Optimizing VLP-QD formation.** All TEM images of VLP-QDs were assembled using 1 mM KCl reassembly buffer and the following conditions: **A)** QD605. **B)** QD605s and uranyl acetate replacement stain C) QD525s and uranyl acetate replacement stain. **D)** closeup of the same conditions as C, *I* points to the

capsid protein shell and *II* points to the QD positioned at its core. Scale bar depicts 20 nm.

Before cellular uptake studies were conducted, a fluorescent microplate assay was performed to assess total fluorescence and provide an estimate of the number of VLP-QD525s present in our sample. The concentration was determined to be $4.17 \times 10^{10}$ VLP/mL (**Figure 2.4**). The standard curve generated used concentrations between $2.46 \times 10^{9}$ NP/mL and $9.6 \times 10^{14}$ NP/mL. A hyperbolic curve was fit to the fluorescence intensity, as the concentration/fluorescence intensity is non-linear, however the actual relationship is unclear ($R^2=1$) [94].

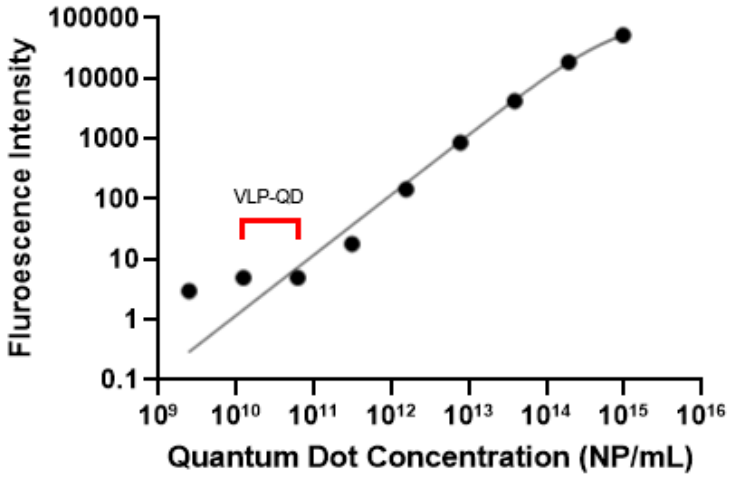


**Figure 2.4: Estimation of VLP-QD concentration.** A hyperbolic curve was used to fit the QD concentrations using the following parameters: $B_{max}=95570$, $K_d=7.976 \times 10^{14}$)

Particles were added, QD525 ($2.4 \times 10^{11}$ QD/mL) or VLP-QD ($2 \times 10^{9}$ VLP/mL), to determine cellular uptake *in vitro*. HEK cells were incubated with QDs or VLP-QDs for 3

hours, washed with PBS, fixed, then imaged. There was no observed fluorescence in the control image (**Figure 2.5A).** Comparable uptake of QDs (**Figure 2.5B**) and VLP-QDs (**Figure 2.5C**) can be seen inside small red vesicles. The QD and VLP-QD look very similar, however there were 100x higher concentration of QD than VLP-QD, indicating that VLP-QD may have utilized receptor-mediated endocytosis rather than passive uptake as they were surrounded by AAV2 capsid protein.

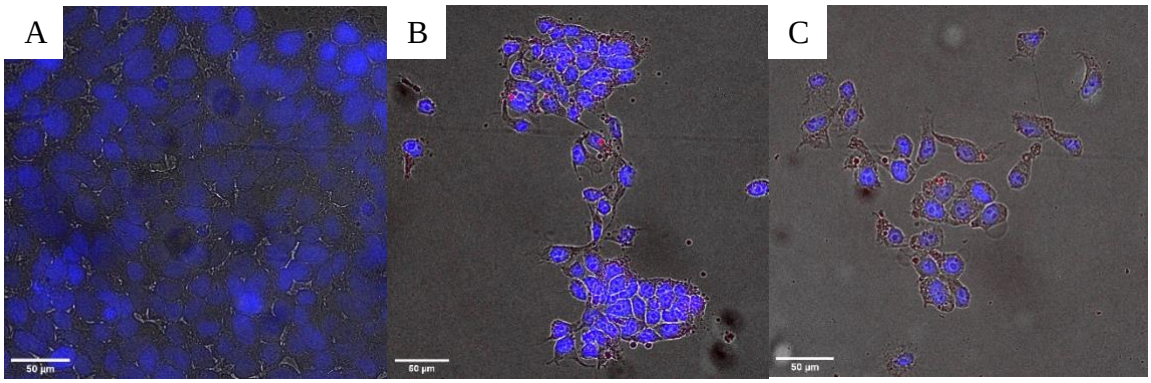


**Figure 2.5: Uptake of VLP-QD. A)** HEK cells stained with Hoechst. **B)** HEK cells stained with Hoechst and incubated with QD525 **C)** HEK cells stained with Hoechst and incubated with VLP-QD525. Scale bars represent 50µm.

## Future Directions

The results of this study demonstrate that formation of VLPs from disassembled AAV2 CPs is possible and that the incorporation of QD525 into the core of these particles can be achieved. The VLP-QD525 particles have the potential to improve the imaging methodologies currently used to assess biodistribution post-administration. However, before this is a real possibility, they must be further characterized to confirm they act sufficiently like AAV2.

Future studies should focus on methods to identify whether the capsid formation of VLP-QD525s is comparable to AAV2, such as an AAV2 titration ELISA, and to confirm which capsid proteins make up the VLP by using immunoprecipitation or fast protein liquid chromatography (FPLC). The AAV2 titration ELISA assay uses the A20 antibody, which only binds to a specific motif found on an intact AAV2 particle. Preliminary ELISAs were inconclusive due to the low absorbance values observed. For initial tests, a 1:5 dilution of the VLP-QD525 sample was used to conserve sample for additional experiments. Had a dilution not been used, the absorbance value may have been within the limit of detection and provided a better estimate of the number of VLP-QDs that had a similar protein structure to the AAV2 capsid. This assay could also be performed on disassembled AAV2 to further confirm successful disassembly.

Immunoprecipitation utilizes antibodies hybridized to a bead to separate a heterogeneous protein sample. In this case, a series of immunoprecipitations could be performed using antibodies that target each AAV2 capsid protein to systematically determine which proteins coexist with QD fluorescence after unassembled materials have been removed. Similar experiments could be performed using FPLC; a commercially available heparin column could be used to determine if VLP-QD525s interact with the same primary receptor as AAV2.

In summary, we have demonstrated that by performing dialysis against simple buffers, AAV2 can be disassembled into protein subunits, reassembled into a VLP, and a QD525 can be inserted into its core. Our results provide evidence that the VLP-QD525s can be up-taken by HEK cells *in vitro*, however further studies are required to determine its primary receptor for cell entry and whether the capsid structure is comparable to AAV2.

# Chapter Three: Diffusion of Extracellular Vesicles through Human Mucus

## Introduction

Recent studies have indicated that extracellular vesicles (EVs) exhibit therapeutic properties and have become appealing in gene therapy and regenerative medicine[95]. The vast majority of these studies rely on the EV cargo from mesenchymal stem cells rather than the loading of a therapeutic. EVs play an important role in intercellular communication in the lungs, which is a good indicator they can move through the complex mucus barrier with ease, however no published studies to date have been done to elucidate this ability. Because of the diversity of cargo that can be loaded into EVs and the fact they are inherently part of the pulmonary immune system, we were interested in exploring their mucus penetrating ability.

Pulmonary diseases such as cystic fibrosis (CF), asthma and chronic obstructive pulmonary disease (COPD) are particularly difficult to treat because of the thick mucus barrier they cause. The standard treatment options are typically inhaled therapies, which have many factors that can be tailored to alter a drug's efficacy, such as size and shape[65]. For an inhaled therapeutic to be effective in the clinic, it must be able to penetrate through mucus. Various inhaled therapies for lung disease have been tested, such as nanoparticles and dendrimers, however, none of these drugs have made it to the clinic[96]. Many of these drugs are made of non-biological materials, whereas EVs are endogenously expressed. Another issue with using exogenous materials is the difficulty of selectively targeting diseased cells opposed to healthy ones. This challenge can potentially be overcome by generating EVs from a cell

line with the same disease[97]. Zhang et al. showed that EVs can deliver siRNA and miRNA into mouse lungs *in vivo,* however experiments were performed on healthy mice, rather than a diseased model[98]. Their targeting potential as well as their loading potential give them promise as a drug delivery system.

CF is caused by one or many mutations to the cystic fibrosis transmembrane regulator (CFTR), a membrane protein that functions as a $Cl^-$ channel. These mutations result in the degradation of the CFTR during transport to the membrane or make it dysfunctional. When CFTR is not actively transporting $Cl^-$, mucociliary clearance is significantly decreased and the mucus buildup is immense. The most common CF mutation is a deletion in phenylalanine 508 (F508del) that causes a trafficking defect in the ion channel. It has been shown *in vitro* that miRNA-16 has the potential to correct this defect and return the CFTR to a semi-functional state[99]. Although miRNA-16 was not delivered via an EV, miRNA can easily be loaded into one by using one of the aforementioned techniques.

Using multiple particle tracking analysis, we investigated the ability for EV derived from human embryonic kidney cells (HEK) or cystic fibrosis bronchial epithelial cells (CFBE) to penetrate mucus taken from healthy patients without lung disease. We hypothesized that EVs derived from CFBE cells would have higher diffusivity in human mucus when compared to EVs derived from HEK cells because even though they originate from a diseased cell line, they originate in the lung and will still portray membrane proteins that allow for efficient movement through mucus. This study aims to be a first step to determining the mucus penetrating properties of two different types of EVs to evaluate their potential use as an inhaled pulmonary nanocarrier.

## Materials and Methods

### *Cell Culture*

All cells were grown in Dulbecco's Modified Eagle's Medium with 10% Fetal Bovine Serum and penicillin/streptomycin.

### *EV Purification*

Cells were grown in T125 flasks. Conditioned media was collected every 24h until confluency was reached. The collected media was stored at 4˚C until 500mL of conditioned media was collected in total. Once 500mL was collected, it was centrifuged at 1,000 x g for 10 minutes to remove detached cells. For all spins, 1-2mL was left in the tube as not to disturb the pellet. The supernatant was transferred to a new tube and was centrifuged again at 2,000 x g for 20min at 4˚C to remove cellular debris and apoptotic bodies. The supernatant was again transferred to a new tube and centrifuged at 10,000 x g for 30min at 4˚C to remove large vesicles. Lastly, the supernatant was transferred to an ultracentrifuge tube and centrifuged at 100,000 x g for 2hr at 4˚C. The supernatant was then removed, and the pellet was carefully reconstituted in 500µL of PBS. The newly resuspended EVs were then placed into a 300kDa ultrafiltration tube and centrifuged at 8,000 x g for 1min at 4˚C. They were then washed with 500µL PBS. After 3 washes total, the purified EVs were resuspended in 500µL PBS. The size and concentration were verified using a Nanosite LM10 using NTA analytical software version 2.4 and BCA assay, respectively.

### *Loading fluorescently labeled miRNA into purified EVs*

Loading miRNA was performed via pH gradient. The EVs (300µg/ml) were first combined with 70% Ethanol and allowed to dehydrate for 12hr in a biological safety cabinet. Next

the dehydrated EVs were rehydrated in citrate buffer, pH 2.5, and placed on a shaker for 1 hr at 25˚C. After 30 min the EVs were resuspended and placed back on the shaker. The EVs were pipetted into dialysis tubing and dialyzed against 1X HBS buffer. The buffer was exchanged every 2 hours, three times, then left overnight. EVs were collected the following morning and were purified using a 100kDa spin filter. They were centrifuge at 3,000 x g for 30min at 4˚C. The sample was resuspended in 300µL of 1X HBS and filtered through a .22µm filter. BCA and NTA analysis were performed to obtain the EV to protein ratio to determine purity. 100µg of EVs were then combined with 1nmol of miRNA and were incubated for 2 hr at 25˚C. The sample was then washed three times using 500µL of PBS using a 300kDa MWCO Nanosep tube (8,000 x g for 15min). EVs were resuspended in 100uL PBS.

*Sample preparation for fluorescent video microscopy*

Slides were prepared by sealing a rubber O-ring on glass slides with vacuum grease. Nanoparticles were sonicated for 30 minutes prior to use. Human mucus was thawed on ice, then 20µL was transferred within the newly formed O-ring well. The sample was incubated at room temperature for 10 minutes to ensure it was no longer chilled. Peg-coated nanoparticles, 0.5µL of ~.002% w/v, were added and mixed into a seperate human mucus sample as a control. EVs used in tracking experiments were concentrated using a 100kDa spin filter and reconstituted in 20µL PBS. 1µL of the concentrated sample was added to 20uL of human mucus which was then stirred. Measurements were collected using a Zeiss 800 LSM microscope equipped with a x63/1.20 W Korr UV VIS IR water-immersion objective and an Axiocam 702 camera with resolution of .093µm/pixel. Images were collected at a frame rate of 33.33 Hz for 10 seconds.

*Particle Tracking Data Analysis*

The particle tracking data analysis is based on previously developed image processing algorithm[100]. An intensity threshold was first set to distinguish the particles from the background, then the eccentricity threshold was set to ensure only spherical particles were selected to distinguish from aggregates or oddly-shaped particles. The centers of the nanoparticles above the brightness threshold and below the eccentricity cutoff are assigned a center based on their (x,y) image location. The centers were then tracked frame by frame allowing for the calculation of their mean-squared displacement (MSD). The average MSD value at 1 second was used to compare diffusion rates between samples.

## Results and Discussion

*Extracellular Vesicle Characterization*

The size distribution and concentration of the extracellular vesicles (EV) was determined using nanoparticle tracking analysis (NTA) before and after pH loading (**Figure 3.1A and B**). The mode diameter was used to best represent the size-population with the highest concentration. The mode diameter for EV derived from HEK cells (HEK-EV) was 139.5±41.3nm compared to 139.5±54.9nm after pH loading (**Figure 3.1C**). The same analysis was also performed on EV derived from CFBE cells (CFBE-EV), whose mode diameter was 165.1±63.8nm before loading and 168.4±100.7nm after loading indicating the loading process had little to no effect on the integrity of the membrane (**Figure 3.1D**).

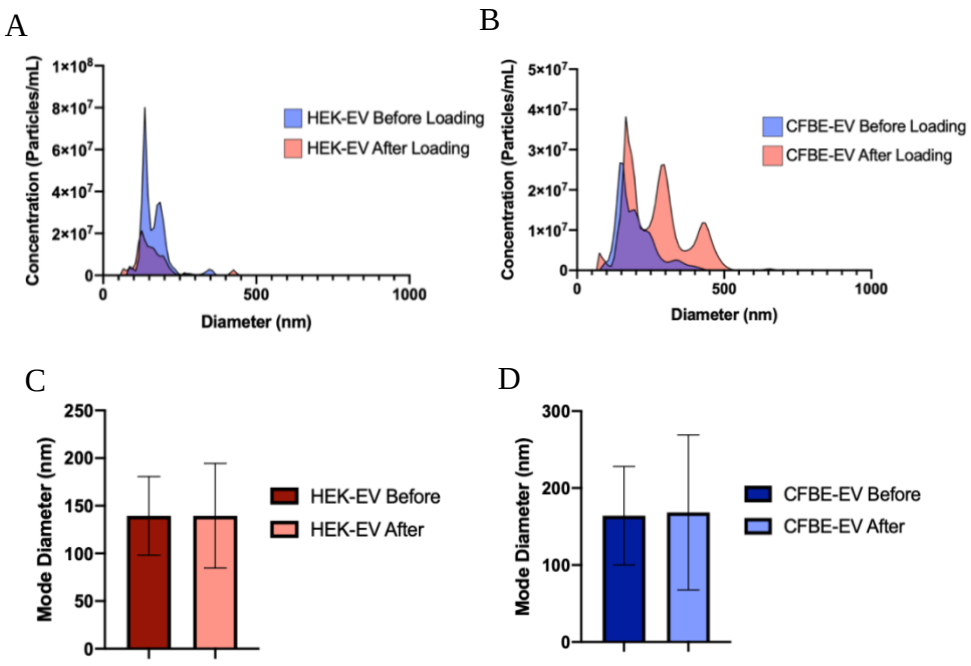


**Figure 3.1: EV size distribution determined by NTA. A) S**ize distribution of HEK-EV before and after loading. **B)** Size distribution of CFBE-EV before and after loading. **C)** Mode diamter of HEK-EV. **D)** Mode diameter of CFBE-EV. All EV characterization experiments were performed by Stephanie Kronstadt in the Jay Lab at University of Maryland.

In the characterization of the concentration and size of the EV it was expected that the concentration would decrease slightly and that the size distribution would remain pretty much constant as we saw with the HEK-EV. The CFBE-EV size distribution shifted larger after loading while the mode diameter remained unchanged. This indicated that there may have been other proteins present in the preparation that led to particle aggregation or that the EV isolation protocol for CFBE-EV had not yet been optimized. It is important to note

that the CFBE-EV come from a diseased cell line with cystic fibrosis (CF), and it has been shown that CF cells produce many more vesicles than other cell lines. This could indicate that means that more strenuous purification measures are required for this particular cell-line that are unnecessary for EV from other cell lines[101].

*Diffusion in Human Mucus*

After NTA characterization, the mobility of HEK-EV and CFBE-EV in human mucus was evaluated using fluorescent video microscopy to measure the MSD of EVs loaded with fluorescently labeled miRNA. The diffusivity of the HEK-EVs was significantly lower than the control particles in each sample **(Figure 3.2A**). In each sample tested with CFBE-EV, there was also significant decrease in diffusivity when compared to the 100nm PEG-coated nanoparticles (**Figure 3.2B**). When the combined logMSD values were compared for all samples, the HEK-EV and CFBE-EV both were significantly less mobile than the control. However, when the HEK-EV and CFBE-EV were directly compared the CFBE-EV had a significantly higher logMSD (**Figure 3.2C**).

The HEK-EV and the CFBE-EV had significantly lower MSD values in each of the mucus samples, however when directly compared, the CFBE-EV were significantly more mobile than the HEK-EV. This indicated that CFBE-EV can diffuse much better, perhaps, because they are derived from lung cells whereas HEK-EVs are derived from kidney cells. Although CFBE-EVs had a higher combined logMSD than the HEK-EVs, the HEK-EV experiments were performed in human mucus with one less freeze-thaw which has been shown to impact the MSD of nanoparticles[100].

Although both HEK-EVs and CFBE-EV had significantly lower MSD than the 100nm-PEG coated particles, it shows that it is possible to improve the mobility of EV in human mucus simply by using a different cell line for EV generation, indicating that the utilization of other lung EVs as drug delivery vehicles is possible. Improvement of EV diffusion through mucus is the next barrier to overcome as the transfer of the CFTR gene *in vitro* has already been demonstrated using EVs derived from Calu-3 and A549[101]. With the improvement of EV loading techniques, miRNA16 could potentially be loaded into EVs as it has been shown to exhibit CFTR restorative properties[97].

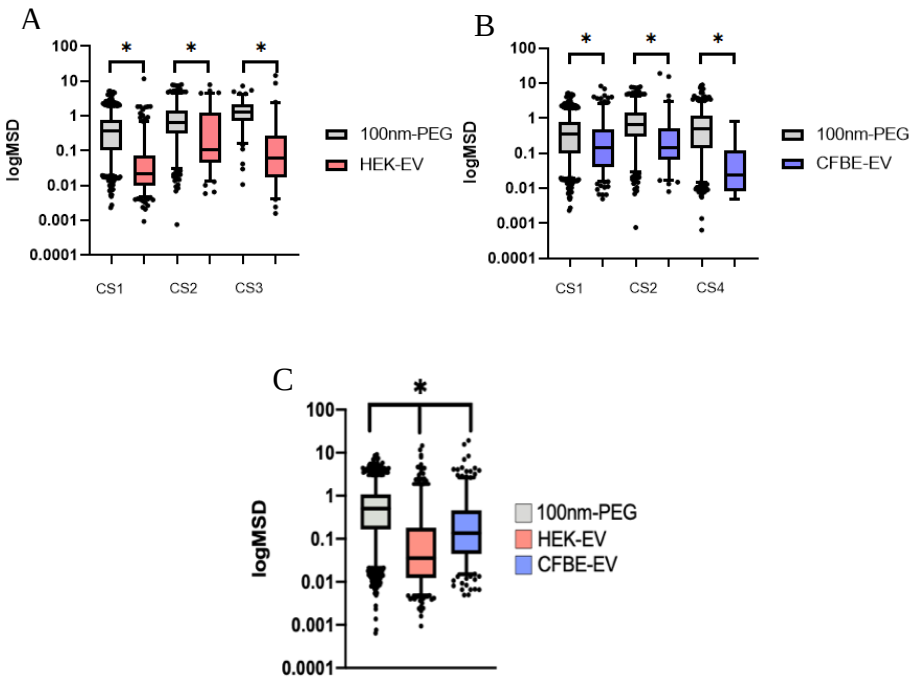


**Figure 3.2: Diffusion of EV in Human Mucus. A)** MSD of HEK-EV in human mucus. **B)** MSD of CFBE-EV in human mucus. Significance was determined using the Mann-Whitney test (*P< 0.0001**). C)** Combined MSD of HEK-EV and CFBE-EV in all human mucus samples. The Kruskal-Wallis test and Dunn's multiple

comparison test were performed to determine significance between the combnined datasets (*P< 0.0001).

## Future Directions

EVs have untapped potential to be effective delivery vectors. Not only are there many other sources of EVs that can be investigated, modifications to their lipid membrane could also be done to improve their ability to move unhindered through the mucus barrier in the lung.

Future experiments should focus on the utilization of air-liquid-interface (ALI) cultures to identify EV populations that can penetrate through the mucus barrier. ALI cultures would provide useful information on protein expression as well as mucus penetration, as similar experiments have been performed using other gene delivery vectors[102]. ALI cultures expressing a diseased phenotype could also be used to identify EVs suited to treat specific mutations. The utilization of QDs into the core of EVs could also be investigated to improve the quality of bioimaging, as this has only recently begun to be explored[102].

This work helped to provide a very basic understanding of EV mobility in human mucus that will hopefully encourage others to investigate different types of EVs further and to explore surface modifications to enhance mobility in complex biological systems.

# Chapter 4: Summery and Conclusions

*Viral-Like-Particle Quantum Dot Encapsulation*

The aim of this work was to improve the labeling methodology of AAV to gain the ability to assess biodistribution directly post-administration *in vivo*. Using current methods, a reporter gene must be expressed before any type of signal can be obtained. This process can take days to weeks, leaving a large window of opportunity for a QD based approach. Here, we engineered VLPs using capsid proteins from AAV2 and encapsulated a QD into their core to combine the immense brightness and photostability of QDs to the broad utility of the AAV vector for gene delivery. By adapting a method that has been demonstrated in other non-enveloped, icosahedral viruses, we showed that it is possible to disassemble intact AAV2 virions and that they can be reassembled using dialysis. This is the first study to date that uses dialysis to demonstrate the disassembly and reassembly of VLPs using AAV capsid proteins.

*Extracellular Vesicle Diffusion through human mucus*

We were interested in investigating EVs mucus penetrating ability. EVs are an endogenously expressed gene delivery vector with largely untapped potential. EVs have been observed to deliver genes *in vitro* however no studies to date have been done to demonstrate their ability to navigate through the human mucus barrier; one that first must be crossed for efficient drug delivery. Here we demonstrated that CFBE-EV could diffuse through human mucus significantly faster than HEK-EV even though the mode diameter of the EV population was slightly larger. These results give good indication that EVs obtained from cells derived from lung epithelia have the ability to penetrate human mucus

significantly better than EV obtained from cells of other origins however further experiments are necessary to fully elucidate their gene delivery capabilities through a mucus barrier.

## References


1. Gao, J. *et al.* In Vivo Tumor-Targeted Fluorescence Imaging Using Near-Infrared Non-Cadmium Quantum Dots. (2010) doi:10.1021/bc900323v.

2. Dixit, S. K. *et al.* Quantum Dot Encapsulation in Viral Capsids. (2006) doi:10.1021/nl061165u.

3. Joo, K. il *et al.* Enhanced real-time monitoring of adeno-associated virus trafficking by virus-quantum dot conjugates. *ACS Nano* **5**, 3523–3535 (2011).

4. Li, H. *et al.* Applications of genome editing technology in the targeted therapy of human diseases: mechanisms, advances and prospects. *Signal Transduction and Targeted Therapy* vol. 5 (2020).

5. Jayant, R. D. *et al.* Current status of non-viral gene therapy for CNS disorders. *Expert Opinion on Drug Delivery* vol. 13 1433–1445 (2016).

6. Goswami, R. *et al.* Gene therapy leaves a vicious cycle. *Frontiers in Oncology* vol. 9 (2019).

7. Elverum, K. & Whitman, M. Delivering cellular and gene therapies to patients: solutions for realizing the potential of the next generation of medicine The Promise and the Challenge. *Gene Therapy* doi:10.1038/s41434-019-0074-7.

8. Naldini, L. Ex vivo gene transfer and correction for cell-based therapies. *Nature Reviews Genetics* vol. 12 301–315 (2011).

9. Mingozzi, F. & High, K. A. Therapeutic in vivo gene transfer for genetic disease using AAV: Progress and challenges. *Nature Reviews Genetics* vol. 12 341–355 (2011).

10. Atchison, R. W., Casto, B. C. & Hammon, W. McD. Adenovirus-Associated Defective Virus Particles. *Science* **149**, 754–755 (1965).

11. Im, D.-S. & Muryczka, N. *The AAV Origin Binding Protein Rep88 Is an ATP-Dependent Site-SpeMic Endcm with DNA Helicase Activity*. *Cell* vol. 61 (1990).

12. King, J. A., Dubielzig, R., Grimm, D. & Kleinschmidt, J. È. R. A. *DNA helicase-mediated packaging of adeno-associated virus type 2 genomes into preformed capsids*. (2001).

13. Myers, M. W. & Carter', B. J. *Assembly of Adeno-Associated Virus*. *VIROLOGY* vol. 102 (1980).

14. Agbandje-McKenna, M. & Kleinschmidt, J. AAV capsid structure and cell interactions. *Methods in Molecular Biology* vol. 807 47–92 (2011).

15. Stahnke, S. *et al.* Intrinsic phospholipase A2 activity of adeno-associated virus is involved in endosomal escape of incoming particles. *Virology* **409**, 77–83 (2011).

16. Xie, Q. *et al.* The atomic structure of adeno-associated virus (AAV-2), a vector for human gene therapy. *Proceedings of the National Academy of Sciences of the United States of America* **99**, 10405–10410 (2002).

17. Keiser, N. W., Yan, Z., Zhang, Y., Lei-Butters, D. C. M. & Engelhardt, J. F. Unique Characteristics of AAV1, 2, and 5 Viral Entry, Intracellular Trafficking, and Nuclear Import Define Transduction Efficiency in HeLa Cells. doi:10.1089/hum.2011.044.

18. Nonnenmacher, M. & Weber, T. Article Adeno-Associated Virus 2 Infection Requires Endocytosis through the CLIC/GEEC Pathway. *Cell Host and Microbe* **10**, 563–576 (2011).

19. Popa-Wagner, R. *et al.* Impact of VP1-Specific Protein Sequence Motifs on Adeno-Associated Virus Type 2 Intracellular Trafficking and Nuclear Entry. *Journal of Virology* **86**, 9163–9174 (2012).

20. Li, C. & Samulski, R. J. Engineering adeno-associated virus vectors for gene therapy. *Nature Reviews Genetics* vol. 21 255–272 (2020).

21. Haberman, R. P., McCown, T. J. & Samulski, R. J. Novel Transcriptional Regulatory Signals in the Adeno-Associated Virus Terminal Repeat A/D Junction Element. *Journal of Virology* **74**, 8732–8739 (2000).

22. McCarty, D. *et al.* Adeno-associated virus terminal repeat (TR) mutant generates self-complementary vectors to overcome the rate-limiting step to transduction in vivo. *Gene Therapy* **10**, 2112–2118 (2003).

23. Hirsch, M. L., Wolf, S. J. & Samulski, R. J. Delivering Transgenic DNA Exceeding the Carrying Capacity of AAV Vectors. *Methods Mol Biol* **18**, 77–83 (2010).

24. Hirsch, M. L. *et al.* Oversized AAV Transductifon Is Mediated via a DNA-PKcs-independent, Rad51C-dependent Repair Pathway. (2013) doi:10.1038/mt.2013.184.

25. Ghosh, A., Yue, Y., Lai, Y. & Duan, D. A hybrid vector system expands adeno-associated viral vector packaging capacity in a transgene-independent manner. *Molecular Therapy* **16**, 124–130 (2008).

26. Nayak, S. & Herzog, R. W. Progress and prospects: Immune responses to viral vectors. *Gene Therapy* vol. 17 295–304 (2010).

27. Calcedo, R., Vandenberghe, L. H., Gao, G., Lin, J. & Wilson, J. M. Worldwide Epidemiology of Neutralizing Antibodies to Adeno-Associated Viruses. *The Journal of Infectious Diseases* **199**, (2009).

28. Zhong, L. *et al. Next generation of adeno-associated virus 2 vectors: Point mutations in tyrosines lead to high-efficiency transduction at lower doses*. www.pnas.org/cgi/content/full/ (2008).

29. Li, C. *et al.* Adeno-associated virus capsid antigen presentation is dependent on endosomal escape. *Journal of Clinical Investigation* **123**, 1390–1401 (2013).

30. Pei, X. *et al.* Efficient Capsid Antigen Presentation From Adeno-Associated Virus Empty Virions In Vivo. *Frontiers in Immunology* **9**, 844 (2018).

31. Mendell, J. R. *et al. Dystrophin Immunity in Duchenne's Muscular Dystrophy*. *N Engl J Med* vol. 363 (2010).

32. Duan, D., Yue, Y., Yan, Z., Yang, J. & Engelhardt, J. F. Endosomal processing limits gene transfer to polarized airway epithelia by adeno-associated virus. *Journal of Clinical Investigation* **105**, 1573–1587 (2000).

33. Nicolson, S. C. *et al.* Identification and Validation of Small Molecules That Enhance Recombinant Adeno-associated Virus Transduction following High-Throughput Screens. (2016) doi:10.1128/JVI.02953-15.

34. Cervelli, T. *et al.* Processing of recombinant AAV genomes occurs in specific nuclear structures that overlap with foci of DNA-damange-response proteins. *Journal of Cell Science* **121**, 349–357 (2008).

35. Schwartz, R. A. *et al.* The Mre11/Rad50/Nbs1 Complex Limits Adeno-Associated Virus Transduction and Replication Downloaded from. *JOURNAL OF VIROLOGY* **81**, 12936–12945 (2007).

36. Grifman, M. *et al.* Incorporation of tumor-targeting peptides into recombinant adeno-associated virus capsids. *Molecular Therapy* **3**, 964–975 (2001).

37. White, S. J. *et al.* Targeted Gene Delivery to Vascular Tissue In Vivo by Tropism-Modified Adeno-Associated Virus Vectors. *Circulation* **109**, 513–519 (2004).

38. Müller, O. J. *et al.* Random peptide libraries displayed on adeno-associated virus to select for targeted gene therapy vectors. *Nature Biotechnology* **21**, 1040–1046 (2003).

39. Chai, Z. *et al.* Application of polyploid adeno-associated virus vectors for transduction enhancement and neutralizing antibody evasion HHS Public Access. *J Control Release* **262**, 348–356 (2017).

40. Zinn, E. *et al.* In silico reconstruction of the viral evolutionary lineage yields a potent gene therapy vector HHS Public Access. *Cell Rep* **12**, 1056–1068 (2015).

41. Perabo, L. *et al.* Combinatorial engineering of a gene therapy vector: Directed evolution of adeno-associated virus. *Journal of Gene Medicine* **8**, 155–162 (2006).

42. Dalkara, D. *et al.* In vivo-directed evolution of a new adeno-associated virus for therapeutic outer retinal gene delivery from the vitreous. *Science Translational Medicine* **5**, 189ra76-189ra76 (2013).

43. Steines, B. *et al.* CFTR gene transfer with AAV improves early cystic fibrosis pig phenotypes. *Anatomy and Cell Biology* **1**, (2016).

44. Wistuba, A. *et al. Subcellular Compartmentalization of Adeno-Associated Virus Type 2 Assembly*. *JOURNAL OF VIROLOGY* vol. 71 (1997).

45. Myers, M. W. & Carter', B. J. *Assembly of Adeno-Associated Virus*. *VIROLOGY* vol. 102 (1980).

46. Bleker, S., Pawlita, M. & Kleinschmidt, J. A. Impact of Capsid Conformation and Rep-Capsid Interactions on Adeno-Associated Virus Type 2 Genome Packaging. *JOURNAL OF VIROLOGY* **80**, 810–820 (2006).

47. Sonntag, F., Schmidt, K. & Kleinschmidt, J. A. A viral assembly factor promotes AAV2 capsid formation in the nucleolus. **107**, (2010).

48. Sonntag, F. *et al.* The Assembly-Activating Protein Promotes Capsid Assembly of Different Adeno-Associated Virus Serotypes. *Journal of Virology* **85**, 12686–12697 (2011).

49. Naumer, M. *et al.* Properties of the Adeno-Associated Virus Assembly-Activating Protein. *13038 jvi.asm.org Journal of Virology* **86**, 23 (2012).

50. Maurer, A. C. *et al.* The Assembly-Activating Protein Promotes Stability and Interactions between AAV's Viral Proteins to Nucleate Capsid Assembly HHS Public Access. *Cell Rep* **23**, 1817–1830 (2018).

51. Earley, L. F. *et al.* Adeno-associated Virus (AAV) Assembly-Activating Protein Is Not an Essential Requirement for Capsid Assembly of AAV Serotypes 4, 5, and 11 Downloaded from. **91**, 1980–1996 (2017).

52. Grosse, S. *et al.* Relevance of Assembly-Activating Protein for Adeno-associated Virus Vector Production and Capsid Protein Stability in Mammalian and Insect Cells. **91**, 1198–1215 (2017).

53. Deroose, C. M. *et al.* Noninvasive Monitoring of Long-Term Lentiviral Vector-Mediated Gene Expression in Rodent Brain with Bioluminescence Imaging. (2006) doi:10.1016/j.ymthe.2006.05.007.

54. Cuillel, M., Berthet-Colominas, C., Timmins, A. & Zulauf, M. *European Biophysics Journal Reassembly of brome mosaic virus from dissociated virus A neutron scattering study*. *Eur Biophys J* vol. 15 (1987).

55. Butler, P. J. G. *Self-assembly of tobacco mosaic virus: the role of an intermediate aggregate in generating both specificity and speed*.

56. McCarthy, M. P., White, W. I., Palmer-Hill, F., Koenig, S. & Suzich, J. A. Quantitative Disassembly and Reassembly of Human Papillomavirus Type 11 Virus like Particles In Vitro. *Journal of Virology* **72**, 32–41 (1998).

57. Hagan, M. F. & Elrad, O. M. Understanding the Concentration Dependence of Viral Capsid Assembly Kinetics-the Origin of the Lag Time and Identifying the Critical Nucleus Size. *Biophysj* **98**, 1065–1074.

58. Yan, D. *et al.* Quantum Dots Encapsulated with Canine Parvovirus-Like Particles Improving the Cellular Targeted Labeling. (2015) doi:10.1371/journal.pone.0138883.

59. Adam Zlotnick. To Build a Virus Capsid. *Molecular Biology* **241**, 59–67 (1994).

60. Li, L. *et al.* Cargo-Compatible Encapsulation in Virus-Based Nanoparticles. (2019) doi:10.1021/acs.nanolett.9b00679.

61. Raposo, G. & Stahl, P. D. Extracellular vesicles: a new communication paradigm? *Nature Reviews Molecular Cell Biology* vol. 20 509–510 (2019).

62. Receptor-mediated endocytosis of transferrin and recycling of the transferrin receptor in rat reticulocytes. *The Journal of Cell Biology* **97**, 329 (1983).

63. Kowal, J., Tkach, M. & Théry, C. Biogenesis and secretion of exosomes. *Current Opinion in Cell Biology* vol. 29 116–125 (2014).

64. Pettersen Hessvik, N. & Llorente, A. Current knowledge on exosome biogenesis and release. *Cellular and Molecular Life Sciences* **75**, 193–208 (2018).

65. Sun, W., Luo, J. D., Jiang, H. & Duan, D. D. Tumor exosomes: A double-edged sword in cancer therapy. *Acta Pharmacologica Sinica* vol. 39 534–541 (2018).

66. Andreu, Z. & Yáñez-Mó, M. Tetraspanins in extracellular vesicle formation and function. *Frontiers in Immunology* **5**, (2014).

67. Doyle, L. & Wang, M. Overview of Extracellular Vesicles, Their Origin, Composition, Purpose, and Methods for Exosome Isolation and Analysis. *Cells* **8**, 727 (2019).

68. Wolfers, J. *et al.* Tumor-derived exosomes are a source of shared tumor rejection antigens for CTL cross-priming. *Nature Medicine* **7**, 297–303 (2001).

69. Hood, J. L., San Roman, S. & Wickline, S. A. Exosomes released by melanoma cells prepare sentinel lymph nodes for tumor metastasis. *Cancer Research* **71**, 3792–3801 (2011).

70. Jayaseelan, V. P. Emerging role of exosomes as promising diagnostic tool for cancer. *Cancer Gene Therapy* 1–4 (2019) doi:10.1038/s41417-019-0136-4.

71. Weber, J. A. *et al.* The MicroRNA Spectrum in 12 Body Fluids. *Clinical Chemistry* **56**, 1733–1741 (2010).

72. Valadi, H. *et al.* Exosome-mediated transfer of mRNAs and microRNAs is a novel mechanism of genetic exchange between cells. doi:10.1038/ncb1596.

73. Carthew, R. W. & Sontheimer, E. J. Origins and Mechanisms of miRNAs and siRNAs. *Cell* vol. 136 642–655 (2009).

74. Rand, T. A., Petersen, S., Du, F. & Wang, X. Argonaute2 cleaves the anti-guide strand of siRNA during RISC activation. *Cell* **123**, 621–629 (2005).

75. Johnsen, K. B. *et al.* Evaluation of electroporation-induced adverse effects on adipose-derived stem cell exosomes. *Cytotechnology* **68**, 2125–2138 (2016).

76. Jeyaram, A. *et al.* Enhanced Loading of Functional miRNA Cargo via pH Gradient Modification of Extracellular Vesicles. *Molecular Therapy* **28**, 975–985 (2020).

77. Ginn, S. L., Amaya, A. K., Alexander, I. E., Edelstein, M. & Abedi, M. R. Gene therapy clinical trials worldwide to 2017: An update. *The Journal of Gene Medicine* **20**, e3015 (2018).

78. Analysis of AAV Serotypes 1â€“9 Mediated Gene Expression and Tropism in Mice After Systemic Injection | Elsevier Enhanced Reader. https://reader.elsevier.com/reader/sd/pii/S1525001616317324?token=7A355D2E5E92A14BBBA5BB8C8444959CF4A890E13E5BF3D89D4A0D883C3419A712A2D6EF313E9AD7A301D7D4B2C192F7.

79. Kaspar, B. K. *et al.* Adeno-associated virus effectively mediates conditional gene modification in the brain. *Proceedings of the National Academy of Sciences of the United States of America* **99**, 2320–2325 (2002).

80. Lux, K. *et al.* Green Fluorescent Protein-Tagged Adeno-Associated Virus Particles Allow the Study of Cytosolic and Nuclear Trafficking. *Journal of Virology* **79**, 11776–11787 (2005).

81. Banin, U., Peng Supported, X., W Chan, W. C. & Nie, S. *Quantum Dot Bioconjugates for Ultrasensitive Nonisotopic Detection Downloaded from*. http://science.sciencemag.org/ (2016).

82. Chen, W. Nanoparticle fluorescence based technology for biological applications. in *Journal of Nanoscience and Nanotechnology* vol. 8 1019–1051 (2008).

83. Yang, Y. B. *et al.* Single Virus Tracking with Quantum Dots Packaged into Enveloped Viruses Using CRISPR. *Nano Letters* **20**, 1417–1427 (2020).

84. Yan, D. *et al.* Quantum Dots Encapsulated with Canine Parvovirus-Like Particles Improving the Cellular Targeted Labeling. (2015) doi:10.1371/journal.pone.0138883.

85. Dixit, S. K. *et al.* Quantum Dot Encapsulation in Viral Capsids. (2006) doi:10.1021/nl061165u.

86. Li, F. *et al.* Viral Coat Proteins as Flexible Nano-Building-Blocks for Nanoparticle Encapsulation. *Small* **6**, 2301–2308 (2010).

87. Li, F. *et al.* Imaging Viral Behavior in Mammalian Cells with Self-Assembled Capsid-Quantum-Dot Hybrid Particles. *Small* **5**, 718–726 (2009).

88. Lee, S., Kim, M. G., Kim, N. & Lee, G. M. Heparan Sulfate Proteoglycan Synthesis in CHO DG44 and HEK293 Cells. *Biotechnology and Bioprocess Engineering* **21**, 439–445 (2016).

89. Simbolo, M. *et al.* DNA Qualification Workflow for Next Generation Sequencing of Histopathological Samples. *PLoS ONE* **8**, e62692 (2013).

90. Melkikh, A. v. & Sutormina, M. I. Model of active transport of ions in cardiac cell. *Journal of Theoretical Biology* **252**, 247–254 (2008).

91. Tagit, O., de Ruiter, M. v, Brasch, M., Ma, Y. & Cornelissen, J. J. L. M. Quantum dot encapsulation in virus-like particles with tuneable structural properties and low toxicity †. (2017) doi:10.1039/c7ra06684h.

92. Qdot Nanocrystals—Section 6.6 | Thermo Fisher Scientific - US. https://www.thermofisher.com/us/en/home/references/molecular-probes-the-handbook/ultrasensitive-detection-technology/qdot-nanocrystal-technology.html.

93. Lee, S. F. & Osborne, M. A. Photodynamics of a Single Quantum Dot: Fluorescence Activation, Enhancement, Intermittency, and Decay. *J. AM. CHEM. SOC* **129**, 8936–8937 (2007).

94. Sakagami, M. In vivo, in vitro and ex vivo models to assess pulmonary absorption and disposition of inhaled therapeutics for systemic delivery. *Advanced Drug Delivery Reviews* vol. 58 1030–1060 (2006).

95. Anderson, C. F., Grimmett, M. E., Domalewski, C. J. & Cui, H. Inhalable nanotherapeutics to improve treatment efficacy for common lung diseases. *Wiley Interdisciplinary Reviews: Nanomedicine and Nanobiotechnology* vol. 12 e1586 (2020).

96. Zhang, D. *et al.* Exosome-Mediated Small RNA Delivery: A Novel Therapeutic Approach for Inflammatory Lung Responses. *Molecular Therapy* **26**, 2119–2130 (2018).

97. Kumar, P. *et al.* MIR-16 rescues F508del-CFTR function in native cystic fibrosis epithelial cells. *Gene Therapy* **22**, 908–916 (2015).

98. Schuster, B. S., Ensign, L. M., Allan, D. B., Suk, J. S. & Hanes, J. Particle tracking in drug and gene delivery research: State-of-the-art applications and methods. *Advanced Drug Delivery Reviews* vol. 91 70–91 (2015).

99. Duncan, G. A., Jung, J., Hanes, J. & Suk, J. S. The mucus barrier to inhaled gene therapy. *Molecular Therapy* vol. 24 2043–2053 (2016).

100. Useckaite, Z. *et al.* Increased extracellular vesicles mediate inflammatory signalling in cystic fibrosis. doi:10.1136/thoraxjnl-2019-214027.

101. Vituret, C. *et al.* Transfer of the Cystic Fibrosis Transmembrane Conductance Regulator to Human Cystic Fibrosis Cells Mediated by Extracellular Vesicles. *Human Gene Therapy* **27**, 166–183 (2016).

102. Zhang, M., Vojtech, L., Ye, Z., Hladik, F. & Nance, E. Quantum Dot Labeling and Visualization of Extracellular Vesicles. doi:10.1021/acsanm.0c01553.